



HAL
open science

The temperature dependence of heavy-ion damage in iron: a microstructural transition at elevated temperatures

Zhongwen Yao, Mike Jenkins, Mercedes Hernández-Mayoral, Mark Kirk

► **To cite this version:**

Zhongwen Yao, Mike Jenkins, Mercedes Hernández-Mayoral, Mark Kirk. The temperature dependence of heavy-ion damage in iron: a microstructural transition at elevated temperatures. *Philosophical Magazine*, 2010, pp.1. 10.1080/14786430903430981 . hal-00592593

HAL Id: hal-00592593

<https://hal.science/hal-00592593>

Submitted on 13 May 2011

HAL is a multi-disciplinary open access archive for the deposit and dissemination of scientific research documents, whether they are published or not. The documents may come from teaching and research institutions in France or abroad, or from public or private research centers.

L'archive ouverte pluridisciplinaire **HAL**, est destinée au dépôt et à la diffusion de documents scientifiques de niveau recherche, publiés ou non, émanant des établissements d'enseignement et de recherche français ou étrangers, des laboratoires publics ou privés.



The temperature dependence of heavy-ion damage in iron: a microstructural transition at elevated temperatures

Journal:	<i>Philosophical Magazine & Philosophical Magazine Letters</i>
Manuscript ID:	TPHM-09-Jul-0317.R1
Journal Selection:	Philosophical Magazine
Date Submitted by the Author:	15-Oct-2009
Complete List of Authors:	Yao, Zhongwen; University of Oxford, Materials Jenkins, Mike; University of Oxford, Materials Hernández-Mayoral, Mercedes; CIEMAT, Division of Materials Kirk, Mark; Argonne National Laboratory, Materials Science Division
Keywords:	radiation damage, in-situ electron microscopy, defect analysis, microstructural characterization
Keywords (user supplied):	
Note: The following files were submitted by the author for peer review, but cannot be converted to PDF. You must view these files (e.g. movies) online.	
video 1.mov Video 2.mov Video 3.mov Video 4.mov Video 5.mov Video 6.mov	

1
2
3
4
5
6
7
8
9
10
11
12
13
14
15
16
17
18
19
20
21
22
23
24
25
26
27
28
29
30
31
32
33
34
35
36
37
38
39
40
41
42
43
44
45
46
47
48
49
50
51
52
53
54
55
56
57
58
59
60



For Peer Review Only

1
2
3 **The temperature dependence of heavy-ion damage in iron: a**
4 **microstructural transition at elevated temperatures**
5

6
7 Z. Yao ^{*}, M. L. Jenkins ^{*1}, M. Hernández-Mayoral ^{**} and M. A. Kirk ^{***}
8

9 ^{*} Department of Materials, University of Oxford, Parks Rd., OX1 3PH

10 ^{**} Division of Materials, CIEMAT Avenida Complutense, 22, 28040-Madrid

11 ^{***} Materials Science Division, Argonne National Laboratory, Argonne, IL 60439
12
13
14
15
16
17
18
19
20
21
22
23
24
25
26
27
28
29
30
31
32
33
34
35
36
37
38
39
40
41
42
43
44
45
46
47
48

49 ¹ Corresponding author: Email: mike.jenkins@materials.ox.ac.uk
50
51
52
53
54
55
56
57
58
59
60

Abstract

We describe a transition in the dislocation microstructure of pure Fe produced by heavy-ion irradiation of thin foils which took place between irradiation temperatures T_{irr} of 300°C and 500°C. At $T_{\text{irr}} \leq 400^\circ\text{C}$, the microstructure was dominated by round or irregular non-edge dislocation loops of interstitial nature and with Burgers vectors $\mathbf{b} = \frac{1}{2}\langle 111 \rangle$, although interstitial $\langle 100 \rangle$ loops were also present; at 500°C only rectilinear pure-edge $\langle 100 \rangle$ loops occurred. At intermediate temperatures there was a gradual transition between the two types of microstructure. At temperatures just below 500°C, mobile $\frac{1}{2}\langle 111 \rangle$ loops were seen to be subsumed by sessile $\langle 100 \rangle$ loops. A possible explanation of these observations is given.

Deleted:

Deleted: a/2

Deleted: a

Deleted: square

Deleted: a

Deleted: a/2

Deleted: a

1. Introduction

It has been long known that the mechanical properties of steels start to degrade at temperatures above about 500°C - a relatively low temperature ($0.42T_m$). According to recent theoretical calculations [1,2], a possible cause of this is an elastic instability, driven by spin fluctuations. This results in a large reduction in the shear stiffness constant $C' = (C_{11} - C_{12})/2$ at the $\alpha \rightarrow \gamma$ phase transition temperature of 912°C, although effects on mechanical properties are manifest at temperatures well below this. The same theory predicts that dislocation loops with Burgers vector $\mathbf{b} = \langle 100 \rangle$ will become relatively more stable with respect to loops with $\mathbf{b} = \frac{1}{2}\langle 111 \rangle$ with increasing temperature.

Deleted: a

Deleted: a/2

In previous papers we have described *in-situ* ion-irradiation experiments which followed the evolution of microstructures in thin foils of pure iron (Fe) and FeCr alloys at irradiation temperatures $T_{\text{irr}} \leq 300^\circ\text{C}$ [3-5] and at 500°C [5]. These experiments provided support for the view that dislocation loops with $\mathbf{b} = \langle 100 \rangle$ increase in stability with temperature. For $T_{\text{irr}} \leq 300^\circ\text{C}$, the microstructures both in pure Fe and in FeCr alloys irradiated with 150 keV Fe^+ ions were dominated by interstitial loops with Burgers vectors $\mathbf{b} = \frac{1}{2}\langle 111 \rangle$. These loops were frequently round or of irregular shape and had significant shear components, and sometimes coalesced into large finger-shaped loops. However, in the same materials irradiated at 500°C, only rectilinear pure-edge interstitial loops with $\mathbf{b} = \langle 100 \rangle$ loops were present.

Deleted: a

Deleted: a/2

Deleted: a

In the present paper this transition in microstructures is explored in more detail in pure Fe. All images and videos included in this paper were recorded under weak-beam diffraction conditions [6]. The weak-beam method of transmission electron microscopy has become an indispensable tool in this area of research (for a review giving full experimental details, see ref. [7]).

2. Experimental method

The materials were the same as those investigated previously (annealed ultra-high purity polycrystalline Fe and a somewhat less pure Fe single crystal – see ref. [3] for details). Full details of specimen preparation and irradiation in the Argonne-IVEM Tandem Facility have been given in a previous paper [3]. Briefly, specimens were electro-polished with minimum exposure to air and introduced immediately into an Hitachi H-9000NAR transmission electron microscope interfaced to an ion implanter. They were then irradiated with 150 keV Fe^+ self ions at temperatures ranging 400°C to 500 °C, with an estimated accuracy of $\pm 10^\circ\text{C}$. We estimate that for this irradiation condition the peak of the damage occurs at a depth of about 28 nm [3]. The regions of foil investigated in the TEM were typically of thickness 30-40 nm, so the damage peak was close to the foil centre. We found in our previous work that in such foils small $\frac{1}{2}\langle 111 \rangle$ dislocation loops were very mobile, and in some foil orientations some of these loops were lost by glide to the foil surfaces under the influence of surface image forces [3-5]. For this reason the single-crystal Fe used in some of the present experiments was spark-cut into slices parallel to the (110) plane in order to obtain TEM specimens with a [110] foil normal. In

Deleted:)

Deleted: The single-crystal Fe was spark-cut into slices parallel to the (110) plane in order to obtain TEM specimens with a [110] foil normal for reasons given in section 3.2.

[foils of this orientation some loop variants have their Burgers vectors in or close to the foil plane, and so cannot easily be lost by glide \(see section 3.3 for details\).](#)

The evolution of radiation damage was followed by dynamic TEM observations under weak-beam diffraction conditions to doses $\leq 2 \times 10^{19}$ ions m^{-2} (~13 dpa). In most of the present experiments irradiations were terminated at a dose of 2 or 3 $\times 10^{18}$ ions m^{-2} (~1.3-2 dpa). Irradiations were paused from time to time to allow detailed characterization of microstructures using standard diffraction-contrast techniques [7]. Similar detailed characterization was performed at the end of the irradiation after specimens had cooled to room temperature.

Formatted: Indent: First line: 18 pt

3. Results

3.1 $T_{irr} = 400^\circ\text{C}$

At doses $< 10^{18}$ ions m^{-2} , the initial damage microstructure was similar to that seen in previous experiments at 300°C. Small dislocation loops, visible as white dots of diameter less than about 5 nm in weak-beam images, appeared within a timescale of a few video frames. Most of these loops were extremely mobile, making large and frequent “hops” in $\langle 111 \rangle$ directions, consistent with $\frac{1}{2}\langle 111 \rangle$ Burgers vectors. The frequencies and amplitudes of hops were much larger than those seen in the same material at 300°C [3] or in the 1-D diffusion of loops seen in similar material under electron irradiation at temperatures $< 400^\circ\text{C}$ [8]. As the irradiation progressed, loops were seen to interact elastically, making coordinated hops and occasionally coalescing into larger loops. This behaviour is illustrated in video 1, which shows damage development under ion irradiation over a dose range 0 - 5 $\times 10^{17}$ ions m^{-2} . The coalescence after irradiation of a string of three $\frac{1}{2}\langle 111 \rangle$ loops into a larger, but still mobile $\frac{1}{2}\langle 111 \rangle$ loop which then rotates on its glide cylinder is shown in video 2, with stills from this video in figure 1. By a dose of 2 $\times 10^{18}$ ions m^{-2} (~1.3 dpa), elastic interactions led to the formation of chains of large (30-50 nm), round loops in thicker areas, reminiscent of those seen at lower irradiation temperatures [3-5] but on a larger scale. The formation of loop chains under irradiation may be viewed dynamically in video 3.

Deleted: a/2

Deleted: a/2

Deleted: a/2

In video 3, it may be seen that a number of loops appeared more gradually and were immobile, and it was surmised that these had $\langle 100 \rangle$ Burgers vectors. A post-irradiation Burgers vector analysis was carried out at the final dose of 2 $\times 10^{18}$ ions m^{-2} , and selected micrographs from this experiment are shown in figure 2. The analysis confirmed that both $\frac{1}{2}\langle 111 \rangle$ and $\langle 100 \rangle$ loops had formed. Large (30-50 nm) loops had Burgers vectors $\mathbf{b} = \frac{1}{2}[1\bar{1}1]$ or $\mathbf{b} = \frac{1}{2}[11\bar{1}]$ (and so were out of contrast in figure 2d) or $\mathbf{b} = [001]$ (and so were out of contrast in figure 2a). Interestingly, no large loops of the other variants were seen in this area. Small (~ 10 nm) loops of each type and variant were also present. The number density of $\langle 100 \rangle$ loops was larger than that of $\frac{1}{2}\langle 111 \rangle$ loops, but on average they were much smaller, so that a majority of point defects was contained in $\frac{1}{2}\langle 111 \rangle$ loops. This will be quantified and discussed later. Stereo experiments showed that large loops were localized towards the foil centre, whilst smaller loops were distributed throughout the foil, regardless of their Burgers vectors. This may be seen in

Deleted: a

Deleted: a/2

Deleted: a

Deleted: a/2

Deleted: a/2

Deleted: a

Deleted: a

Deleted: a/2

Deleted: a/2

video 4, which shows a tilt series constructed using EM3D tomography software from a set of 7 stereo images taken over a tilt range of $\sim 35^\circ$ with $\mathbf{g} = 002$.

By inspection of figure 2 it may be seen that the large $[001]$ loops are of pure-edge type. The foil normal in this micrograph is $[100]$ and edge-on loops with $\mathbf{b} = [001]$ are seen to lie perpendicular to the diffraction vector $\mathbf{g} = 00\bar{2}$ in figure 2c. Similar pure-edge $\langle 100 \rangle$ loops were found in our previous work at $T_{\text{irr}} = 500^\circ\text{C}$, where their nature was determined to be interstitial [5]. Micrographs taken at other orientations showed that $\langle 100 \rangle$ loops larger than about 20nm were rectilinear with edges along $\langle 100 \rangle$ directions. Smaller ones looked more rounded. The detailed shape of loops is discussed in a separate paper [9].

The $\frac{1}{2}\langle 111 \rangle$ loops are non-edge. A full Burgers vector analysis (carried out using the reflections available at both the $[110]$ and $[100]$ poles) showed that the predominant Burgers vector of the large loops in the area of foil shown in figure 3a was $\frac{1}{2}[\bar{1}11]$. The habit plane of these loops was found by tilting the foil from pole $[110] \rightarrow [310] \rightarrow [100]$, whilst maintaining the same weak-beam diffraction condition with $\mathbf{g} = 002$. The loops appear edge-on at the $[310]$ pole, imaging as lines lying perpendicular to the $[\bar{1}32]$ direction (figure 3a). They therefore lie on or close to the $(\bar{1}32)$ plane, so that the angle between the loop normal \mathbf{n} and \mathbf{b} is about 22° . Figures 3b and 3c show experimental images of two loops recorded close to the $[110]$ and $[310]$ poles respectively. Image simulations using the program TEMACI [10] for circular loops with $\mathbf{b} = \frac{1}{2}[\bar{1}11]$ with a $(\bar{1}32)$ habit plane are inset at the lower left of each figure. The good match between experimental and simulated images confirms our interpretation. In our previous experiments in UHP-Fe at 300°C the large $\frac{1}{2}\langle 111 \rangle$ “finger” loops which formed at high doses were also found to have significant shear components and were also found to be interstitial [4].

3.2 $T_{\text{irr}} = 450^\circ\text{C}$

In an experiment carried out at $T_{\text{irr}} = 450^\circ\text{C}$ on an UHP Fe foil oriented about 20° from $[111]$, early stages in damage development were similar to those seen at 400°C , except that larger-scale microstructures appeared more slowly. Small loops were seen early in the irradiation, and were extremely mobile, and were frequently lost from the foil. As the dose increased, again chains of loops formed, interacting elastically. By a dose of 3×10^{18} ions m^{-2} , long lines of large $\frac{1}{2}\langle 111 \rangle$ loops had formed in thicker regions, all with the same Burgers vector, and looking similar to the microstructure examined in detail at 400°C (figure 4a). In an adjacent grain tilted close to $[100]$, regions were found where large loops of both $\langle 100 \rangle$ and $\frac{1}{2}\langle 111 \rangle$ types were present (figure 4b), although $\langle 100 \rangle$ loops were in a preponderance. In other regions of this grain large numbers of edge-on $\langle 100 \rangle$ loops were visible (figure 4c). The absence of $\frac{1}{2}\langle 111 \rangle$ loops in figure 4c may well be a contrast effect: the large loops in figure 4b are visible in $\mathbf{g} = 01\bar{1}$ and so have either $\mathbf{b} = \frac{1}{2}[\bar{1}11]$ or $\mathbf{b} = \frac{1}{2}[\bar{1}1\bar{1}]$, but loops with these Burgers vectors would be out of contrast in figure 4c which was taken in $\mathbf{g} = 011$. The average sizes of $\langle 100 \rangle$ loops were significantly larger than at 400°C , and a majority of point-defects was now contained in

Deleted: a

Deleted: a

Deleted: a

Deleted: a

Deleted: a/2

Deleted: a/2

Deleted: a/2

Deleted: a/2

Deleted: a/2

Deleted: a

Deleted: a/2

Deleted: a

Deleted: a

Deleted: a/2

Deleted: a/2

Deleted: a/2

Deleted: a

such loops, see below. This temperature seems to mark a transition from a mostly $\frac{1}{2}\langle 111 \rangle$ microstructure to a microstructure dominated by $\langle 100 \rangle$ loops.

Deleted: a

Deleted: a

3.3. $T_{irr} = 460^\circ C - 500^\circ C$

Deleted: 2

At $500^\circ C$, we found in our previous work that only $\langle 100 \rangle$ loops formed in [100] foils [5]. These loops appeared slowly over several minutes, and were immobile. Figure 5a shows the microstructure at a dose of 3×10^{18} ions m^{-2} , where loops of sizes up to about 50 nm were present but well separated. As these loops grew under continuing irradiation, they coalesced with neighbouring loops with the same Burgers vector until they impinged on loops of the other variants, forming the microstructure seen in figure 5b. In this figure, loops belonging to all three $\langle 100 \rangle$ variants can be seen. Two variants, with $\mathbf{b} = [001]$ and $\mathbf{b} = [010]$, appear edge-on, forming a quasi-regular ladder-like structure. Loops of the third variant, with $\mathbf{b} = [100]$, lie in the plane of the foil and are faintly visible in residual $\mathbf{g} \cdot \mathbf{b} \times \mathbf{u}$ contrast. Occasionally during irradiation loops with this Burgers vector were suddenly lost from the foil by glide, see video 5, demonstrating that $\langle 100 \rangle$ loops are not intrinsically sessile.

Deleted: a

Deleted: a

Deleted: a

Deleted: a

Deleted: a

Deleted: a

In foils with normal [100], all variants of $\frac{1}{2}\langle 111 \rangle$ loops have a component of Burgers vector pointing towards the surface. Since $\frac{1}{2}\langle 111 \rangle$ loops are highly mobile at $500^\circ C$, the possibility exists that such loops do form, but are lost by glide to the surface before they are seen. Total loss of $\frac{1}{2}\langle 111 \rangle$ loops in (100) foils is known to occur in ion-irradiated Mo [11]. In order to exclude this possibility, the following experiments were carried out in single-crystal foils with orientation close to [110]. In such foils, loops with $\mathbf{b} = \frac{1}{2}[1\bar{1}1]$ and $\mathbf{b} = \frac{1}{2}[1\bar{1}\bar{1}]$ have little or no component of Burgers vector towards the surface, and so cannot easily be lost by glide.

Deleted: a/2

Deleted: a/2

Deleted: expected to be

Deleted: a/2

Deleted: a/2

Deleted: a/2

First a foil was irradiated to a moderate dose (1×10^{18} m^{-2}) at $500^\circ C$. Sessile loops with $\mathbf{b} = \langle 100 \rangle$ were seen to form, but no loops with $\mathbf{b} = \frac{1}{2}\langle 111 \rangle$ loops were found². A further irradiation of the same foil was then performed at $482^\circ C$. A few small $\frac{1}{2}\langle 111 \rangle$ loops were produced in the field of view of the CCD camera. All remained in the foil and hopped along $\langle 111 \rangle$ directions in the plane of the foil. Soon after irradiation, none of these $\frac{1}{2}\langle 111 \rangle$ loops could be found. It was not clear by which mechanism they had disappeared.

Deleted: a

Deleted: a/2

Deleted: a/2

Deleted: a/2

A second foil was irradiated at $465^\circ C$. Video 6 shows this specimen under ion irradiation, and figure 6 shows a series of stills from this video. The video shows directly the fate of $\frac{1}{2}\langle 111 \rangle$ loops at elevated temperatures. In the area of observation are some easily-recognized, large, sessile, near edge-on $\langle 100 \rangle$ loops and two small (~ 5 nm) $\frac{1}{2}\langle 111 \rangle$ loops, located on either side of a larger (~ 50 nm) $\langle 100 \rangle$ loop (arrowed in figure 6). At first, the two $\frac{1}{2}\langle 111 \rangle$ loops hopped parallel to their Burgers vector. Their glide cylinders did not intersect the $\langle 100 \rangle$ loop. However, within a minute both $\frac{1}{2}\langle 111 \rangle$ loops had moved towards the $\langle 100 \rangle$ loop, this motion involving sideways steps perpendicular to their glide cylinders. On reaching the $\langle 100 \rangle$ loop they were subsumed, causing the

Deleted: a/2

Deleted: a

Deleted: a/2

Deleted: a

Deleted: a/2

Deleted: a

Deleted: a/2

Deleted: a

Deleted: a

² We have recently found the same result in a [110] Fe-C alloy irradiated at $500^\circ C$ under the same conditions.

$\langle 100 \rangle$ loop to grow. The increase in size of the $\langle 100 \rangle$ loop indicates that the two $\frac{1}{2}\langle 111 \rangle$ loops which it had absorbed had the same nature as the $\langle 100 \rangle$ loop itself, i.e. all were interstitial.

Deleted: a

Deleted: a

Deleted: a/2

Deleted: a

4. Discussion

The occurrence of $\langle 100 \rangle$ loops in Fe irradiated at high temperature has been known since the pioneering work of Masters [12], who carried out thin-foil irradiation experiments similar to our own. Masters found exclusively $\langle 100 \rangle$ loops of interstitial nature in pure Fe irradiated with 150keV Fe^+ ions at 550°C. Subsequently $\langle 100 \rangle$ loops, or a mixture of $\langle 100 \rangle$ and $\frac{1}{2}\langle 111 \rangle$ loops, have been found in many other elevated-temperature experiments in ferritic materials. These include, for example, experiments by Konobeev *et al* [13] who found $\langle 100 \rangle$ interstitial loops (as well as voids) in Fe and Fe 0-18%Cr irradiated with fast neutrons to doses up to 25.8 dpa at 400°C. As a further example, Gelles [14] also found that $\langle 100 \rangle$ loops predominated in Fe3%Cr alloys irradiated with neutrons to ~ 20dpa at temperatures between 400°C and 450°C, although a mixture of the two loop types was found in higher Cr alloys. In our own recent experiments in Fe irradiated in the bulk with 0.5-3 MeV Fe^+ ions to ~ 10 dpa at 500°C, we also found almost exclusively interstitial $\langle 100 \rangle$ loops, whilst at 300°C a mixture of $\langle 100 \rangle$ and $\frac{1}{2}\langle 111 \rangle$ loops was present. In FeCr alloys, however, both loop types were present at 500°C [15]. In these and other experiments there does seem a clear pattern for $\langle 100 \rangle$ loops to predominate in pure Fe at irradiation temperatures $T_{\text{irr}} \geq 400^\circ\text{C}$. In contrast, in Fe irradiated at 60°C with neutrons, only $\frac{1}{2}\langle 111 \rangle$ loops were identified, again of interstitial nature [16]. The only examples we know of $\langle 100 \rangle$ loops in low-temperature irradiations are found in Fe irradiated with W^+ ions at room temperature [17] and with high doses of self-ions [18], and in these cases loops were considered to have formed by a process of cascade collapse and the loop nature was *vacancy*.

Deleted: a

Deleted: a

Deleted: a

Deleted: a

Deleted: a/2

Deleted: a

Deleted: a

Deleted: a

Deleted: a

Deleted: a/2

Deleted: a

Deleted: a/2

Deleted: a

Our present work has provided further evidence that $\langle 100 \rangle$ loops become increasingly dominant in Fe with increasing irradiation temperature. In figure 7 we have made an attempt to quantify the proportions of interstitials contained in $\langle 100 \rangle$ and $\frac{1}{2}\langle 111 \rangle$ at various temperatures. This figure was constructed by measuring the size distributions and number densities of the two types of loops at different irradiation temperatures. At $T_{\text{irr}} = 400^\circ\text{C}$, about 80% of loops were of the $\langle 100 \rangle$ type, but their mean size was only about a third that of the $\frac{1}{2}\langle 111 \rangle$ loops, and so the fraction of interstitials contained in loops of the two types was comparable. At $T_{\text{irr}} = 450^\circ\text{C}$, the majority of interstitials was contained in $\langle 100 \rangle$ loops, but large $\frac{1}{2}\langle 111 \rangle$ round loops were still present in some areas. At $T_{\text{irr}} \geq 492^\circ\text{C}$, no $\frac{1}{2}\langle 111 \rangle$ loops were seen during ion irradiation, whereas $\langle 100 \rangle$ loops formed and grew. As a rough estimate, the total number of interstitials contained in $\langle 100 \rangle$ loops at 500°C was comparable with the number of interstitials contained in loops at 300°C, for the same irradiation dose. No correction has been made in figure 7 for loss of mobile $\frac{1}{2}\langle 111 \rangle$ loops to the surface, nor for the effects of foil orientation and thickness, nor for the variability in loop types from area to area. Discussions of these effects may be found in our previous papers [3,5]. Their neglect is likely to lead to an underestimate of the number of interstitials in $\frac{1}{2}\langle 111 \rangle$ loops at all temperatures, but we believe that the trends shown are real.

Deleted: a

Deleted: a

Deleted: a/2

Deleted: a

Deleted: a/2

Deleted: a

Deleted: a/2

Deleted: a

Deleted: a

Deleted: a

Deleted: a/2

Deleted: a/2

In parallel with our experimental work, Dudarev *et al.* [1,2] developed methods of calculating the self-energy of loops of different Burgers vectors and morphologies as a function of temperature. As mentioned in the introduction, they found that the reduction in the shear stiffness constant C' with increasing temperature caused a profound effect on the anisotropic elastic self-energies of dislocations in Fe and on the relative stability of $\langle 100 \rangle$ and $\frac{1}{2}\langle 111 \rangle$ dislocation loops. For example, for loops of perimeter $P = 10$ nm, hexagonal, prismatic pure-edge dislocation loops with Burgers vector $\frac{1}{2}\langle 111 \rangle$ were found to be unconditionally stable at temperatures $T < 350^\circ\text{C}$, whereas square $\langle 100 \rangle$ pure-edge loops were unconditionally stable for $T > 550^\circ\text{C}$. In the intermediate temperature region, $350^\circ\text{C} < T < 550^\circ\text{C}$, loops of this size with $\mathbf{b} = \frac{1}{2}\langle 111 \rangle$ and edges along $\langle \bar{1}10 \rangle$ directions were thermodynamically unstable and could lower their free energy either by changing shape (with edges along $\langle 11\bar{2} \rangle$ directions) or by transforming to $\langle 100 \rangle$ loops. Dudarev *et al.* [2] argued that in a real situation where loops of various sizes and shapes are present, the boundaries between the different regions of stability would be diffuse, leading to a gradual transition in loop types.

This picture above is clearly in good qualitative accord with our observations. We found that $\frac{1}{2}\langle 111 \rangle$ loops were dominant components of the microstructure at temperatures $T_{\text{irr}} \leq 300^\circ\text{C}$, although small $\langle 100 \rangle$ loops were present even at room temperature [3,4]. At temperatures $T_{\text{irr}} \geq 400^\circ\text{C}$, $\langle 100 \rangle$ loops became increasingly important components of the microstructure (figure 7). Our observations are therefore compatible with a picture that $\langle 100 \rangle$ loops become more energetically favoured with increasing temperature. However the mechanism by which the transition in loop types takes place is still not entirely clear. In particular, the abrupt disappearance of $\frac{1}{2}\langle 111 \rangle$ loops at temperatures $T_{\text{irr}} > 465^\circ\text{C}$ was something of a surprise. Unlike Arakawa *et al* [19] we did not see $\frac{1}{2}\langle 111 \rangle$ loops transform directly into $\langle 100 \rangle$ loops. Small mobile $\frac{1}{2}\langle 111 \rangle$ loops were produced at $T_{\text{irr}} = 465^\circ\text{C}$, but were quickly subsumed by sessile $\langle 100 \rangle$ loops. The crabwise motion by which the $\frac{1}{2}\langle 111 \rangle$ loops approached the $\langle 100 \rangle$ loop (video 6, figure 6) evidently involved self-climb, since the sizes of the $\frac{1}{2}\langle 111 \rangle$ loops remained unchanged at the resolution of the CCD camera. Coalescence of interstitial loops by self-climb has been observed previously during an isothermal anneal of ion-implanted UO_2 by Turnbull [20]. Turnbull considered two possible driving forces: first the mutual interaction of the loop strain fields, and second the interaction of the strain fields of loops and vacancies. He concluded that in metals both interactions were likely to be important.

Clues to the possible mechanisms underlying our observations may be gleaned from molecular dynamics simulations of displacement cascades in Fe by Bacon and co-workers [21]. In these simulations small self-interstitial clusters formed at the cascade peripheries at the end of the displacement phase of the cascade in an essentially athermal process, or by short-range diffusion during the thermal-spike phase. Smaller clusters may be considered as bundles of $\langle 111 \rangle$ or $\langle 100 \rangle$ crowdions. These clusters are very mobile, even at low temperatures, moving by thermally-activated one-dimensional glide along the crowdion direction. Larger clusters of crowdions may be considered as small, but probably sub-microscopic $\frac{1}{2}\langle 111 \rangle$ or $\langle 100 \rangle$ dislocation loops. We surmise that loops large enough to be seen in the TEM form by the coalescence of such small clusters, and

Deleted: a

Deleted: a/2

Deleted: a/2

Deleted: a

Deleted: a/2

Deleted: a

Deleted: a/2

Deleted: a

Deleted: a

Deleted: a

Deleted: a/2

Deleted: a/2

Deleted: a

Deleted: a/2

Deleted: a

Deleted: a/2

Deleted: a

Deleted: a/2

Deleted:

Deleted: Most

Deleted: a/2

that this process is more likely to occur in the foil interior since the surfaces act as efficient sinks. Loops with $\mathbf{b} = \langle 100 \rangle$ which reach visible size become sessile, whereas $\mathbf{b} = \frac{1}{2}\langle 111 \rangle$ loops remain mobile. Both types continue to grow by absorbing mobile submicroscopic clusters and smaller loops, and by coalescing with loops of comparable size. In the case of the mobile $\frac{1}{2}\langle 111 \rangle$ loops, elastic interactions play an important role in this process. The relative proportions of the two loop types are probably determined by by a combination of factors, including their stabilities at small sizes, and the increased mobility of $\frac{1}{2}\langle 111 \rangle$ loops at higher temperatures. At temperatures above 450°C, small $\frac{1}{2}\langle 111 \rangle$ loops are less likely to form, and those which do are quickly subsumed into $\langle 100 \rangle$ loops and never reach large sizes. At temperatures higher than 500°C this process may occur before any microscopic $\frac{1}{2}\langle 111 \rangle$ loops form at all, and so such loops are not seen in the high temperature regime.

Deleted: a

Deleted: a/2

Deleted: a/2

Deleted: a/2

Deleted: a

Deleted: s

Deleted: a/2

A final question concerns the fate of vacancies in our experiments. We have determined the nature of larger loops using the inside-outside contrast technique, and all were found to be interstitial. Evidence presented in this paper shows that most if not all of the mobile $\frac{1}{2}\langle 111 \rangle$ loops are also interstitial in nature. Vacancy-rich regions are likely to form within cascades, but calculations suggest that closed vacancy loops of size $\leq 4\text{nm}$ are not formed, while small open loops transform to voids [22,23]. We have looked for but not found small voids in pure Fe, suggesting that any present are of size below the resolution limit of $\sim 2\text{nm}$. We did find very small voids in Fe8%Cr irradiated under similar conditions [5]. It is also possible that some of the small near-surface loops might be of vacancy nature [3].

Deleted: a/2

5. Summary and conclusions

- We have described a transition in the microstructures of pure Fe produced by heavy-ion irradiation of thin foils which took place between irradiation temperatures T_{irr} of 300°C and 500°C.
- Our previous work had shown that for $\leq 300^\circ\text{C}$, the microstructure was dominated by interstitial loops with Burgers vectors $\mathbf{b} = \frac{1}{2}\langle 111 \rangle$. At $T_{\text{irr}} = 400^\circ\text{C}$, about 50% of self-interstitials were still contained in $\frac{1}{2}\langle 111 \rangle$ loops, which were frequently round or of irregular shape and had shear components. These loops were very mobile and frequently coalesced into larger loops. A high proportion of small, sessile, edge $\langle 100 \rangle$ loops was also present, also accommodating about 50% of the interstitials.
- There was a gradual transition in microstructure at temperatures greater than 400°C. At $T_{\text{irr}} = 450^\circ\text{C}$, loops with $\mathbf{b} = \frac{1}{2}\langle 111 \rangle$ were still present, and interacted elastically to form long chains, but loops with $\mathbf{b} = \langle 100 \rangle$ of pure edge character and rectilinear shape, now dominated in most areas, and accommodated a majority of the interstitials.

Deleted: a/2

Deleted:

Deleted: a/2

Deleted: a

Deleted: a/2

- At temperatures $T_{irr} \geq 450^\circ\text{C}$, small, mobile $\frac{1}{2}\langle 111 \rangle$ loops were seen to be subsumed by sessile $\langle 100 \rangle$ loops, and large $\frac{1}{2}\langle 111 \rangle$ loops did not form. At 500°C , $\langle 100 \rangle$ loops developed into large networks, and no visible $\frac{1}{2}\langle 111 \rangle$ loops formed.
- A plausible explanation of these observations has been given in terms of the relative stabilities of $\frac{1}{2}\langle 111 \rangle$ and $\langle 100 \rangle$ loops as a function of temperature, and the possible mechanism by which the microstructure develops.

Deleted: a/2

Deleted: a/2

Deleted: a/2

Deleted: a/2

Deleted: a

Acknowledgements

We thank Dr. A. Liu and P. Baldo of Argonne National Lab for their help in using this facility. The IVEM-Tandem Facility (within the Electron Microscopy Center at ANL) is supported by the US DOE Office of Science and operated under contract no. DE-AC02-06CH11357 by UChicago Argonne, LLC. We are grateful to Dr. S. L. Dudarev and Dr. S. P. Fitzgerald for helpful discussions. We thank B. Miller, D. Graham, and Prof. I M. Robertson (UIUC) for help with video 4. Part of this work was funded by the UKAEA, Culham Science Centre.

References

1. S. P. Fitzgerald and S. L. Dudarev, Proc. R. Soc. A **464** 2549 (2008).
2. S. L. Dudarev, R. Bullough and P. M. Derlet, Phys. Rev. Lett., **100** 135503 (2008).
3. Z. Yao, M. Hernandez-Mayoral, M. L. Jenkins and M.A. Kirk, Phil. Mag. **88** 2851 (2008).
4. M. Hernandez-Mayoral, Z. Yao, M. L. Jenkins and M.A.Kirk, Phil. Mag. **88** 2881 (2008).
5. M. L. Jenkins, Z. Yao, M. Hernandez-Mayoral and M. A. Kirk, J. Nucl. Mat. **389** 5 (2009).
6. D. J. H. Cockayne, I. L. F. Ray and M. J. Whelan, Phil. Mag, **20** 1265 (1969).
7. M. L. Jenkins and M. A. Kirk (2001), Characterisation of Radiation Damage by Transmission Electron Microscopy, Institute of Physics Series in Microscopy in Materials Science (Series Editors, B Cantor and M J Goringe) ISBN 0 7503 0748 X (hbk)
8. K. Arakawa, K. Ono, M. Isshiki, K. Mimura, M. Uchikoshi and H. Mori, Science p.956, 318 (2007)
9. S. Fitzgerald and Z. Yao, Phil. Mag. Lett. (2009), in press.
10. Z. Zhou, M. L. Jenkins, S.L. Dudarev, A. Sutton and M. A. Kirk, Phil. Mag **86** 4851 (2006).
11. C. A. English and M. L. Jenkins, Phil. Mag. (2009), in press.
12. B. C. Masters, Phil. Mag. **11** 881 (1965).
13. Y. Konobeev, A. Dvoriashin, S. Porollo and F. Garner, J. Nucl. Mat. **355** 9 (2005).
14. D. Gelles, J Nucl. Mat. **108-9** 515 (1982).
15. S. Xu, Z. Yao and M.L. Jenkins, J. Nucl. Mat. (2009) in press.
16. B. L. Eyre and A. F. Bartlett, Phil. Mag. **12** 261 (1965).
17. M. L. Jenkins, C. A. English and B. L. Eyre, Phil. Mag. **38** 97 (1978).

- 1
- 2
- 3 18. M. A. Kirk., I. M. Robertson, M. L. Jenkins, C. A. English, T. J. Black and J. S.
- 4 Vetrano, *J. Nucl. Mat.* **149** 21 (1987).
- 5 19. K. Arakawa, M. Hatanaka, E. Kuramoto, K. Ono, and H. Mori, *PRL* **96** 125506
- 6 (2006)
- 7 20. J. A. Turnbull, *Phil. Mag.* **21** 83 (1970).
- 8 21. D. J. Bacon, F. Gao and Y. Osetsky, *J. Nucl. Mat.* **276** (2000).
- 9 22. M. R. Gilbert, S. L. Dudarev, P. M. Derlet and D. G. Pettifor, *J. Phys: Condens.*
- 10 *Matter* **20** 345214 (2008).
- 11 23. M. R. Gilbert, Z. Yao, M. L. Jenkins and S. L. Dudarev, *J. Nucl. Mat.* **386-8** 36
- 12 (2009).
- 13
- 14
- 15
- 16
- 17
- 18
- 19
- 20
- 21
- 22
- 23
- 24
- 25
- 26
- 27
- 28
- 29
- 30
- 31
- 32
- 33
- 34
- 35
- 36
- 37
- 38
- 39
- 40
- 41
- 42
- 43
- 44
- 45
- 46
- 47
- 48
- 49
- 50
- 51
- 52
- 53
- 54
- 55
- 56
- 57
- 58
- 59
- 60

For Peer Review Only

Figure captions

Figure 1: Frames captured from video 2, showing loop coalescence in UHP Fe after irradiation at 400°C to 1×10^{18} ions m^{-2} . This occurred soon after ion irradiation ceased, as the specimen was being examined in the TEM and was still at 400°C. Three small $\frac{1}{2}\langle 111 \rangle$ loops towards the centre of frame A coalesce into a single $\frac{1}{2}\langle 111 \rangle$ loop in frame B. The loop is seen to rotate to new habit plane, frame C, and continues to hop.

Deleted: a/2

Deleted: a/2

Figure 2: Contrast experiment at $T_{irr} = 400^\circ C$ in UHP Fe irradiated to a dose of 2×10^{18} ions m^{-2} (~1.3 dpa): (a) diffraction vector $\mathbf{g} = 020$, so loops with $\mathbf{b} = [100]$ are out of contrast; (b) $\mathbf{g} = 01\bar{1}$, so loops with $\mathbf{b} = \frac{1}{2}[\bar{1}11]$ and $\mathbf{b} = \frac{1}{2}[11\bar{1}]$ are out of contrast; (c) $\mathbf{g} = 00\bar{2}$, so loops with $\mathbf{b} = [010]$ are out of contrast; (d) $\mathbf{g} = 0\bar{1}\bar{1}$, so loops with $\mathbf{b} = \frac{1}{2}[1\bar{1}1]$ and $\mathbf{b} = \frac{1}{2}[\bar{1}1\bar{1}]$ are out of contrast.

Deleted: a

Deleted: a/2

Deleted:

Deleted: a/2

Deleted: a

Deleted: a/2

Deleted: a/2

Deleted: a/2

Deleted: a

Deleted: a

Deleted: a/2

Deleted: a/2

Deleted: a/2

Deleted: a/2

Chains of $\frac{1}{2}\langle 111 \rangle$ loops are present together with a few large $[001]$ loops and a large number of small loops of both types. In this field of view $\langle 001 \rangle$ loops outnumber $\frac{1}{2}\langle 111 \rangle$ loops about in a ratio of about 2:1.

Figure 3: Experiment to determine the habit plane of $\frac{1}{2}[\bar{1}11]$ loops: (a) the specimen shown in figure 3 has been tilted close to the $[310]$ pole. Loops with $\mathbf{b} = \frac{1}{2}[\bar{1}11]$ appear edge-on on, consistent with a $(\bar{1}32)$ habit plane; (b) and (c) show experimental images of a two loops with $\mathbf{b} = \frac{1}{2}[\bar{1}11]$ at the $[110]$ and $[310]$ poles respectively. TEMACI image simulations for a circular loop with this Burgers vector lying on $(\bar{1}32)$ are inset at the lower left in each case.

Figure 4: Loops in UHP Fe at 450°C at a dose of 3×10^{18} ions m^{-2} : (a) long lines of large $\frac{1}{2}\langle 111 \rangle$ loops in a grain oriented about 20° from $[111]$; (b) large loops of both types in an adjacent grain oriented close to $[001]$, with $\langle 100 \rangle$ loops in a preponderance; (c) edge-on $\langle 100 \rangle$ loops in the same grain.

Deleted: a/2

Deleted: a

Figure 5: Formation of $\langle 100 \rangle$ loops in an $[001]$ foil at 500°C: (a) at a dose of 3×10^{18} ions m^{-2} (b) the same area at a dose of 1×10^{19} ions m^{-2} .

Deleted: a

Figure 6: Stills extracted from video 6, showing single crystal $[110]$ Fe under irradiation at 465°C. The large loop at the centre of the micrograph with $\mathbf{b} = \langle 100 \rangle$ subsumes two smaller $\frac{1}{2}\langle 111 \rangle$ loops.

Deleted: a

Deleted: a/2

Figure 7: Estimates of the fraction of interstitials contained in loops of the two types. The error bars do not take account of systematic errors due to loss of $\frac{1}{2}\langle 111 \rangle$ loops to the surface.

Deleted: a/2

List of videos

Video 1 Early-stage damage development in UHP Fe irradiated at 400°C. Viewed at 2 × real-time.

Video 2 Coalescence of three $\frac{1}{2}\langle 111 \rangle$ loops at 400°C under electron irradiation. Viewed in real-time.

Deleted: a/2

Video 3 Elastic interaction of $\frac{1}{2}\langle 111 \rangle$ loops to form loop chains at 400°C under ion irradiation. Viewed at 30 × real-time.

Deleted: a/2

Video 4 A tilt series reconstruction, showing large loops lie close to the foil centre.

Video 5 Loss of large $[001]$ loops under ion irradiation in an $[001]$ foil at 500°C. Viewed at 10 × real-time.

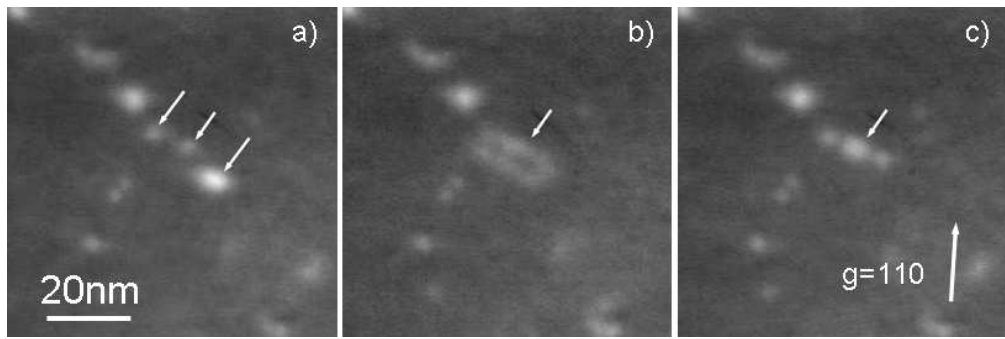
Deleted: a

Video 6 A large $\langle 100 \rangle$ loop subsumes two small $\frac{1}{2}\langle 111 \rangle$ loops under ion irradiation at 465°C. Viewed at 2 × real-time.

Deleted: a

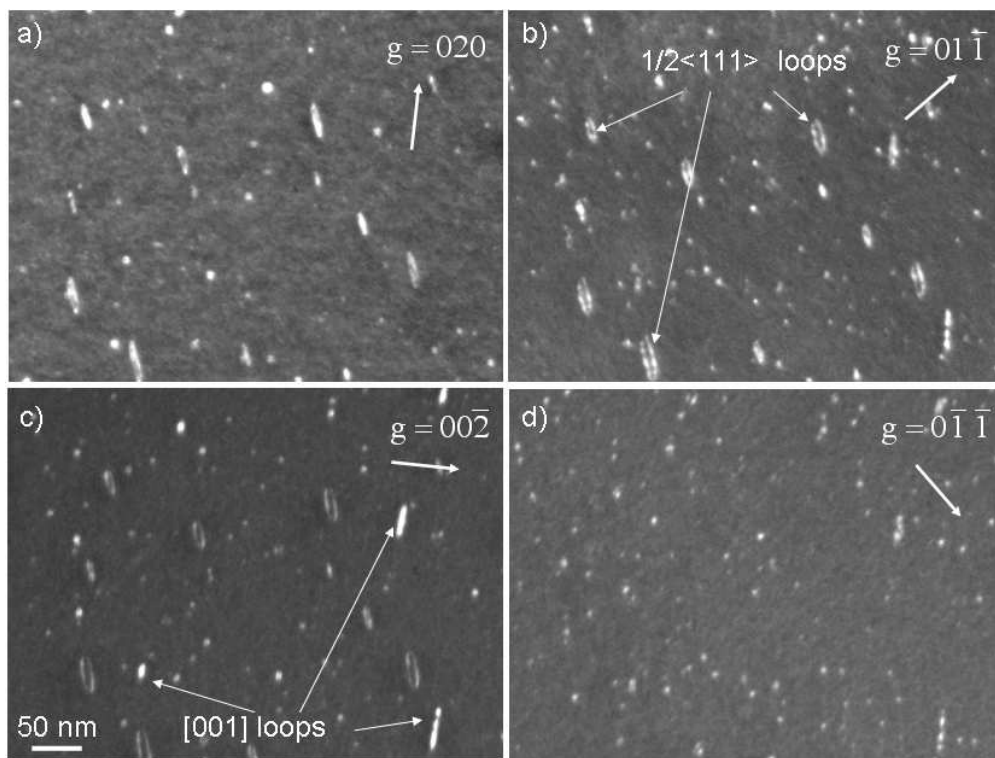
Deleted: a/2

1
2
3
4
5
6
7
8
9
10
11
12
13
14
15
16
17
18
19
20
21
22
23
24
25
26
27
28
29
30
31
32
33
34
35
36
37
38
39
40
41
42
43
44
45
46
47
48
49
50
51
52
53
54
55
56
57
58
59
60



286x94mm (72 x 72 DPI)

Peer Review Only

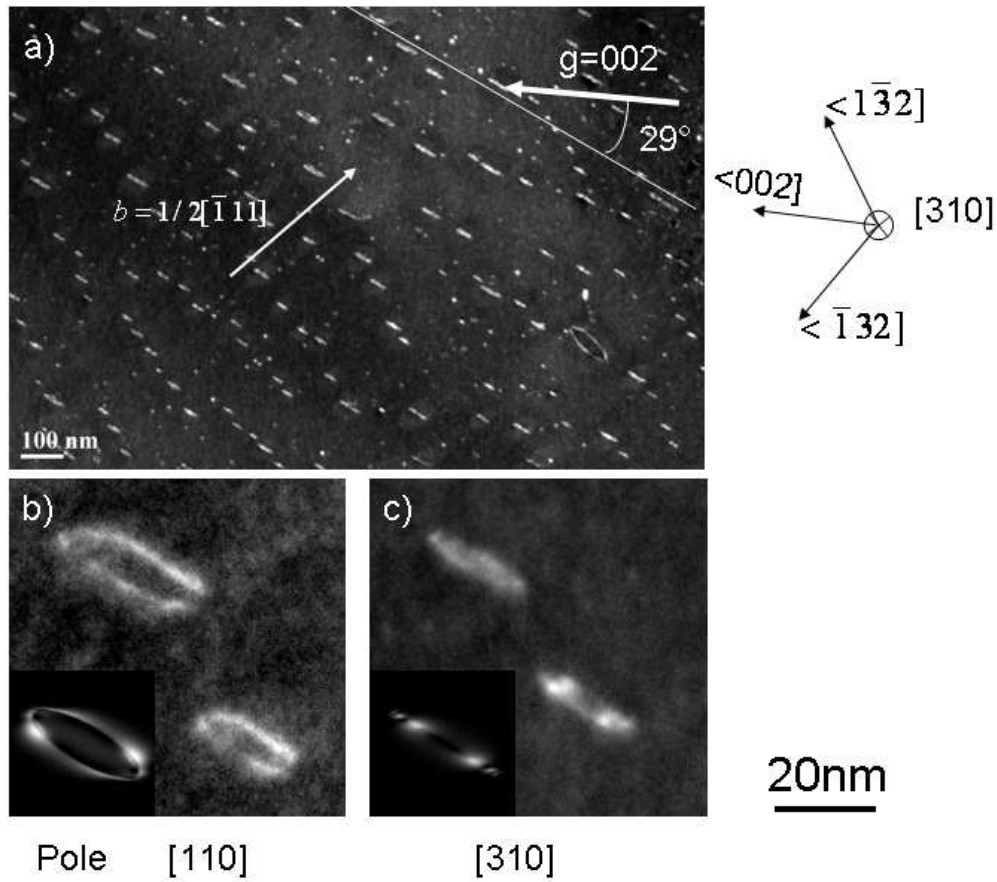


292x220mm (72 x 72 DPI)

View Only

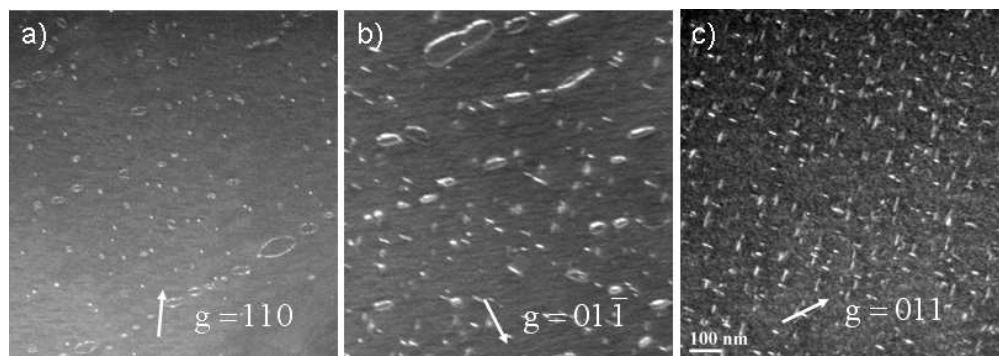
1
2
3
4
5
6
7
8
9
10
11
12
13
14
15
16
17
18
19
20
21
22
23
24
25
26
27
28
29
30
31
32
33
34
35
36
37
38
39
40
41
42
43
44
45
46
47
48
49
50
51
52
53
54
55
56
57
58
59
60

1
2
3
4
5
6
7
8
9
10
11
12
13
14
15
16
17
18
19
20
21
22
23
24
25
26
27
28
29
30
31
32
33
34
35
36
37
38
39
40
41
42
43
44
45
46
47
48
49
50
51
52
53
54
55
56
57
58
59
60



237x209mm (72 x 72 DPI)

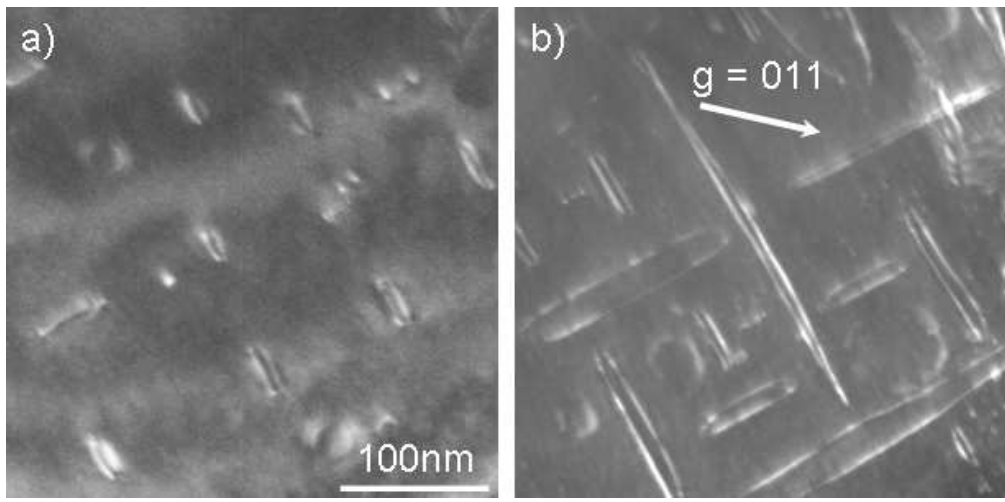
Only



286x100mm (72 x 72 DPI)

Peer Review Only

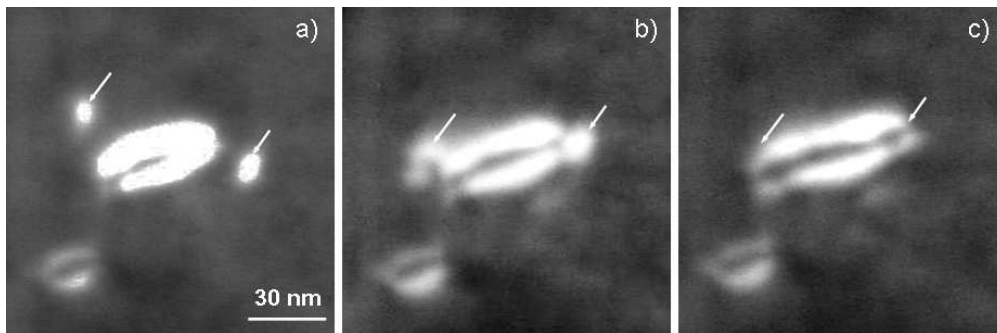
1
2
3
4
5
6
7
8
9
10
11
12
13
14
15
16
17
18
19
20
21
22
23
24
25
26
27
28
29
30
31
32
33
34
35
36
37
38
39
40
41
42
43
44
45
46
47
48
49
50
51
52
53
54
55
56
57
58
59
60



215x105mm (72 x 72 DPI)

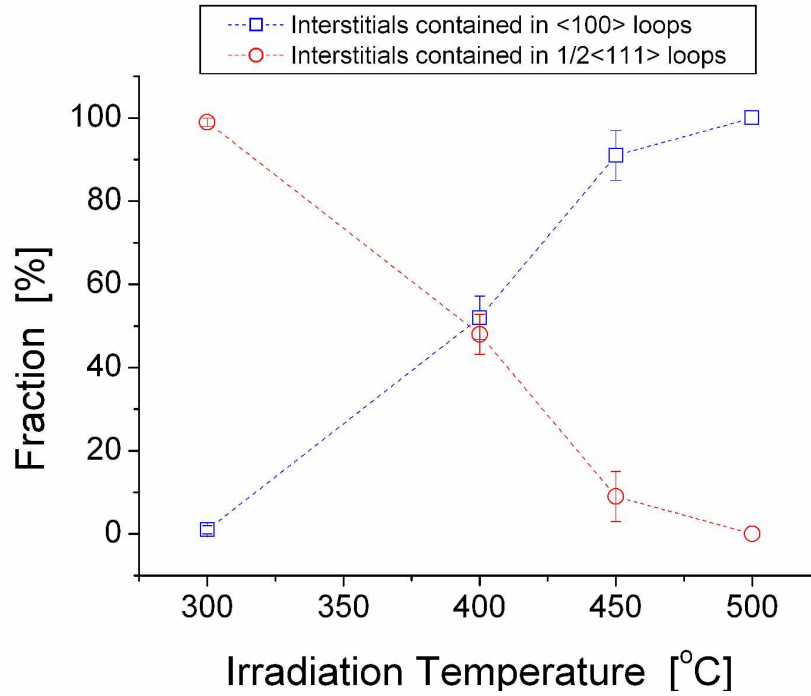
Review Only

1
2
3
4
5
6
7
8
9
10
11
12
13
14
15
16
17
18
19
20
21
22
23
24
25
26
27
28
29
30
31
32
33
34
35
36
37
38
39
40
41
42
43
44
45
46
47
48
49
50
51
52
53
54
55
56
57
58
59
60



325x106mm (72 x 72 DPI)

Peer Review Only



575x399mm (150 x 150 DPI)

View Only